Journal of Materials Chemistry A

ROYAL SOCIETY OF CHEMISTRY

PAPER

View Article Online
View Journal | View Issue

Cite this: J. Mater. Chem. A, 2025, 13, 12977

New pyroelectric figures of merit for harvesting dynamic temperature fluctuations†

Bastola Narayan,[a] Qingping Wang, *[ab] James Roscow,[a] Chaoying Wan [c] and Chris Bowen[a]

Received 24th January 2025
Accepted 25th March 2025

DOI: 10.1039/d5ta00704f

rsc.li/materials-a

Pyroelectric materials are attracting increasing attention for a variety of applications including thermal imaging, thermal sensing, and energy harvesting. To select and design pyroelectric materials with optimal performance, figures of merit (FoMs) are utilized in terms of energy, voltage, and current sensitivity. However, existing FoMs do not take into account heat transfer parameters, such as thermal conductivity and thermal diffusivity. To address this challenge, this paper formulates new performance figures of merit for the selection and design of pyroelectric materials for harvesting dynamic temperature fluctuations. The new figures of merit are of interest for the selection of pyroelectric materials, the design of new materials, or the creation of novel composites for pyroelectric applications, in particular when there is a need for rapid thermal cycles to increase the frequency of operation and maximize the power output for thermal harvesting. High performance materials based on the new figures of merit are highlighted and evaluated, and comparisons between the material classes are discussed, including polycrystalline ceramics, single crystal materials, polymers, thin films, composites and 2D materials. Potential future high-performance pyroelectric materials for thermal harvesting are outlined.

1. Introduction

To address the energy demand in our modern society, two primary strategies have often been considered: reducing energy consumption through enhanced energy efficiency, or expanding our energy production. There is also growing interest in the development self-powered sensors and systems, to mitigate against the challenges associated with the management of the power delivery to a large number of discrete sensors. Energy harvesting has therefore emerged as a critical area of research focus, since it aims to address key challenges related to sustainability, technological innovation, our escalating global energy needs, and the need for continuous sensing and monitoring.

Among the range of available energy harvesting technologies, thermal energy harvesting using pyroelectric materials has attracted interest in an attempt to capture and reuse waste heat.[1] These materials have been produced as macroscopic devices that consist of pyroelectric sensors, energy harvesters and detectors.[2,3] The power levels of these devices are often relatively low, where a common aspect is the low frequency of the thermal cycles; there is therefore a clear need to increase the maximum thermal excitation frequency, or maximise the volume of material that can exhibit a specific thermal cycle.

Pyroelectric materials, as a specialized subset of dielectric materials, exhibit a spontaneous polarization that changes with temperature to generate electrical charge. This unique property enables a pyroelectric material to convert thermal fluctuations into electrical energy, making them a promising solution for waste heat harvesting,[4–7] in particular when there are large and/or rapid changes in temperature.[8] The pyroelectric effect is also employed in thermal sensing, where the charge, current, or voltage, generated as a result of a temperature change in used for thermal imaging and infrared detection, including person/body heat sensors, and fire detectors.[9,10] These fascinating materials also offer possibilities in X-ray generation,[11] neutron generation,[12] pyro-electrocatalytic disinfection,[13] hydrogen production,[14] and electrocaloric cooling.[15]

The origin of the pyroelectric effect stems from a change in the electric dipole moment, namely the polarisation, of a polar material with temperature. As an example, an increase in temperature excites the ions that constitute the dipole moment to a higher energy level in the potential well, thereby changing the mean equilibrium position in the lattice and the resulting dipole moment.[16] There are generally two approaches to changing the temperature of a pyroelectric material to stimulate the dipole and generate an electrical charge, current or a voltage.

[a]Centre of Integrated Materials, Processes and Structures (IMPS), Department of Mechanical Engineering, University of Bath, Bath, BA2 2ET, UK. E-mail: qw608@bath.ac.uk

[b]Department of Physics & Mechanical and Electronic Engineering, Hubei University of Education, Wuhan 430205, P. R. China

[c]International Institute for Nanocomposites Manufacturing (IINM), WMG, University of Warwick, CV4 7AL, UK

† Electronic supplementary information (ESI) available. See DOI: https://doi.org/10.1039/d5ta00704f

The first approach relates to subjecting the pyroelectric material to a temperature shift from one steady state temperature (T_1) to another temperature (T_2), leading to a change in temperature ($\Delta T = T_2 - T_1$) and a change in polarisation (ΔP) to produce electric charge at the surface of the material, thereby converting thermal to electrical energy. An example of such an approach is repeatedly placing a pyroelectric element in a high temperature (T_1) and low temperature (T_2) source, such as a hot and cold liquid[6,17,18] and waiting for the pyroelectric to reach thermal equilibrium. An alternative approach involves the continuous variation of the temperature of a pyroelectric material over time using an oscillating heat source that induces a temperature–time function to generate a change in temperature (dT/dt). This is of interest when heat is generated cyclically at a relatively high frequency; examples include a fluctuating radiation thermal source, such as the intensity of sunlight which fluctuates due to natural processes such as the presence of moving clouds,[19] or heat produced by high-speed electronic switches for computing and data transmission.[20]

While a number of performance figures of merit exist[1,9] for thermal sensing, imaging and harvesting, there are currently no performance figures of merit that take into account the limits imposed due to thermal phenomena and the time–temperature thermal response of a pyroelectric element, such as the thermal conductivity (λ) or thermal diffusivity (K). These parameters are of interest since, intuitively, they can improve the rate of change in temperature and provide a limit to the maximum achievable operating frequency in terms of thermal cycling. Methods to enhance the heat transfer have included patterning the surface of the pyroelectric to improve the absorption of incident radiation[21,22] or combining a pyroelectric with plasmonic nanomaterials.[19,23] However, less attention has been given to the design and selection of the pyroelectric material in terms of their heat transfer parameters.

Before outlining new figures of merit that take into account the ability of a materials to achieve rapid thermal cycles, it is necessary to first outline the range of existing pyroelectric-related figures of merit.

2. Pyroelectric effect and existing figures of merit (FoMs)

Fig. 1 is a schematic of the pyroelectric effect, where we will consider a pyroelectric thermal harvester polarised through its thickness, with electrically conductive electrode located on its upper and lower surfaces. Initially the pyroelectric material is at a temperature (T_1) and is at electrostatic equilibrium since the polarisation of the material is balanced by surface screening charges on the upper and lower electrode surfaces located normal to the polarisation direction, see Fig. 1a. An increase in the temperature of a pyroelectric material ($dT/dt > 0$) to T_2, as shown in Fig. 1b, leads to a reduction in spontaneous polarisation due to an enhanced dipole oscillation. This, in turn, triggers electron migration and current flow (I) in an external circuit to establish a new electrostatic equilibrium, as seen in Fig. 1c. In contrast, when the pyroelectric element is cooled ($dT/dt < 0$), the spontaneous polarisation of the pyroelectric increases, therefore disturbing the electrical equilibrium and inducing reverse electron migration, so that current flows in the opposite direction,[1] Fig. 1d, to establish to new state of equilibrium. Since pyroelectric charge is generated by a change in temperature, the power output is naturally also varying time, where the current will change direction during each heating and cooling cycle. As with a piezoelectric energy harvester the output is therefore AC in nature, and some form of rectification is typically required to provide a DC output, or store the electrical energy.[1] The pyroelectric coefficient (p, units of $C\,m^{-2}\,K^{-1}$) quantifies the pyroelectric effect by measuring the capacity of a material to modify its polarisation intensity (P_s), and produce electrical charge (Q), in response to a change in temperature. The pyroelectric coefficient of an unclamped material, under a constant stress and electric field is defined by eqn (1),[1]

$$p^{\sigma,E} = \left(\frac{dP_s}{dT}\right)_{\sigma,E} \quad (1)$$

where P_s is the spontaneous polarisation, and the superscripts σ and E correspond to the conditions of constant stress and electric field, respectively. It is of interest to note that pyroelectric coefficients are generally negative in sign, since an increase in temperature usually leads to a decrease in polarisation.

Under short-circuit conditions, the resulting pyroelectric electric current (I_{sc}) generated by a pyroelectric material with an electrode area (A) can be determined from,[1]

$$I_{sc} = \frac{dQ}{dt} = pA\frac{dT}{dt} \quad (2)$$

where dT/dt denotes the rate of temperature change. Eqn (2) shows that the short circuit current is proportional to the pyroelectric coefficient (p), rate of change in temperature (dT/dt) and the electrode area of the pyroelectric material (A); it is not dependent on its thickness or volume.

2.1 Pyroelectric figures of merit (FoMs) for thermal sensing

A variety of FoMs have been developed for thermal sensing using pyroelectric materials, with the most popular being the pyroelectric *current sensitivity* (F_i), *voltage sensitivity* (F_V), and *detectivity* (F_D), which are now defined.

A pyroelectric current can be used for sensing changes in temperature, and the relevant figure of merit regarding the current responsivity (F_i) for a given thermal input can be expressed as:[24]

$$F_i = \frac{p}{\rho c_p} = \frac{p}{c_E} \quad (3)$$

where $c_E = \rho c_p$ is the volume specific heat ($J\,m^{-3}\,K^{-1}$), c_p is specific heat capacity ($J\,kg^{-1}\,K^{-1}$) and ρ is the density ($kg\,m^{-3}$) of the pyroelectric material. The F_i figure of merit aims to maximise the current of the sensor generated for a given thermal input, when operating under closed circuit conditions.

The voltage generated can also be used for thermal sensing, where the pyroelectric *voltage sensitivity* (F_V) can be written as:[25]

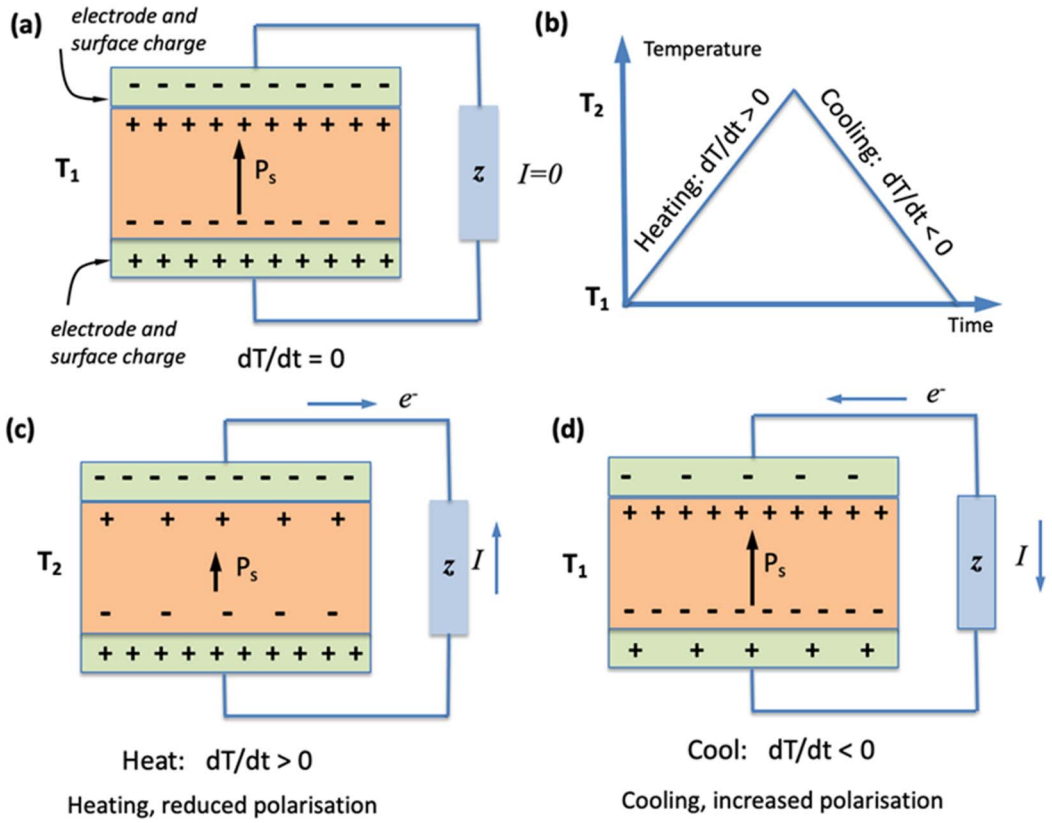

Fig. 1 Schematic of the pyroelectric effect (a) initial state, dT/dt = 0, where current I = 0, (b) heating profile, (c) heating cycle (dT/dt > 0) leads to a decrease in polarisation and current flow, (d) cooling cycle (dT/dt < 0) leads to an increase in polarisation and current flow in opposite direction.

$$F_V = \frac{p}{\rho c_p \varepsilon_{33}^{\sigma}} = \frac{p}{c_E \varepsilon_{33}^{\sigma}} \quad (4)$$

where $\varepsilon_{33}^{\sigma}$ is the permittivity at constant stress (F m^{-1}). The voltage sensitivity, F_V, aims to maximise the voltage generated by the pyroelectric sensor for a given thermal input when operating under open circuit conditions.

An additional figure of merit for pyroelectric-based thermal detection also considers the impact of Johnson noise,[16] by including the dielectric loss (tan δ) of the pyroelectric material in the specific *detectivity* figure of merit:

$$F_D = \frac{p}{c_E(\varepsilon_{33}^{\sigma} \times \tan\delta)^{1/2}} \quad (5)$$

A final voltage-based pyroelectric sensing figure of merit has been developed that aims to minimise lateral thermal diffusion of heat for high special frequencies in the image, by including the thermal diffusivity of the pyroelectric:[1]

$$F_{VlD} = \frac{p}{c_E \varepsilon_{33}^{\sigma} K} \quad (6)$$

where K is the thermal diffusivity, and $K = \frac{\lambda}{\rho c_p} = \frac{\lambda}{c_E}$,[26] In this case, a low thermal diffusivity reduces the lateral diffusion of heat in pyroelectric detector.

For a thermal detector, the figures of merit shown in eqn (3)–(6) are employed to enable effective materials or materials design to maximise device performance. The ideal pyroelectric material in this regard should have (i) a low specific heat to produce a large change in temperature for a given thermal input, (ii) a high pyroelectric coefficient to maximise the charge generated for a given dT/dt, (iii) a low dielectric loss, and (iv) a low dielectric permittivity to maximise the voltage output for a given level of charge. A low thermal diffusivity (K) also reduces lateral diffusion of heat for detectors.

The pyroelectric sensing figures of merit, eqn (3)–(6) are related to the generated voltage or current. However, a current or voltage in isolation does not provide an indication of the electrical energy (or potential power), and is therefore unsuitable for energy harvesting applications, where the generation of energy, power or assessing the overall efficiency of converting thermal energy to electrical energy are important criteria.

2.2 Pyroelectric figures of merit for thermal energy harvesting

For pyroelectric energy harvesting applications, the pyroelectric element usually operates in one of two different modes. For example, it can (i) cycle between two specific temperatures, T_1 and

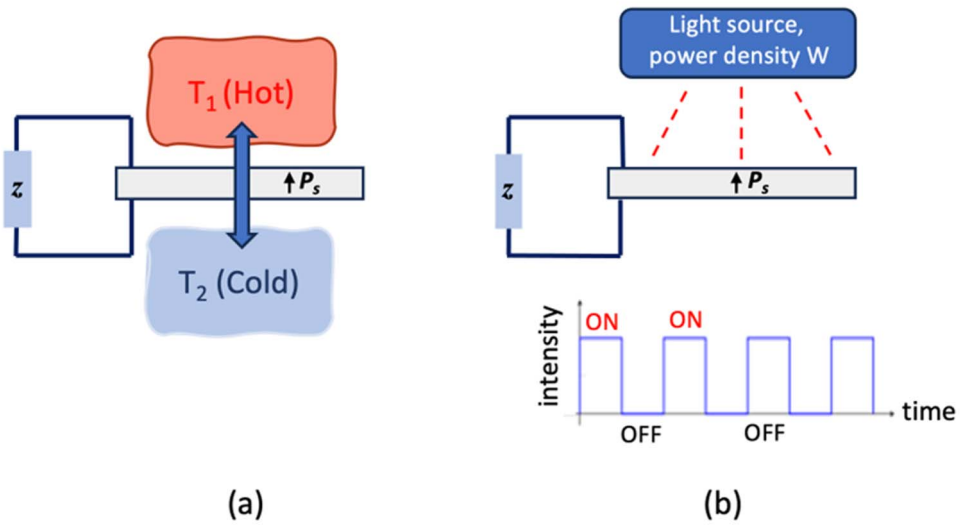

Fig. 2 (a) Cycling between two temperatures, T_1 and T_2, (b) modulated heat source, leading to temperature fluctuations where the final temperature of the pyroelectric material depends on the heat capacity of the material.

T_2 (*e.g.* of hot and cold source), as in Fig. 2a, or (ii) is exposed to an incident heat source that modulates its output and provides a specific power density, W, as in Fig. 2b; in this case the final temperature change of the pyroelectric is dependent on specific heat capacity of the material for a given thermal input.

Two examples of the figures of merit for thermal harvesting using pyroelectrics have been proposed.[27,28] Firstly, an electrothermal coupling factor (k) has been defined to estimate the efficiency of thermal harvesting when cycling between two temperatures, as shown in eqn (7): [27]

$$k^2 = \frac{p^2 T_{\text{hot}}}{\rho c_p \varepsilon_{33}^{\sigma}} = \frac{p^2 T_{\text{hot}}}{c_E \varepsilon_{33}^{\sigma}} \tag{7}$$

where T_{hot} is the maximum working temperature.

A pyroelectric energy-harvesting figure of merit, F_E, has also been proposed as:[28]

$$F_E = \frac{p^2}{\varepsilon_{33}^{\sigma}} \tag{8}$$

and has been used for the selection and design of pyroelectric materials for energy harvesting applications.[6,29–31]

It is of interest to note that compared to the voltage (F_v) and current (F_i) responsivities, the energy harvesting figure of merit, F_E, does not include the volume heat capacity since it is based on cycling between two specific temperatures (*e.g.* T_1 and T_2), rather than a given thermal input (which is the case for thermal imaging applications). To assess the energy generated for a given thermal input, a modified figure of merit (F_E') was recently derived which is the product of F_i (eqn (3)) and F_V (eqn (4)), expressed as:[32]

$$F_E' = F_V F_i = \frac{p^2}{\varepsilon_{33}^{\sigma} \rho^2 {c_p}^2} = \frac{p^2}{\varepsilon_{33}^{\sigma} {c_E}^2} \tag{9}$$

3. New pyroelectric FoMs for harvesting dynamic temperature fluctuations

The figures of merit derived above for energy harvesting (eqn (8) and (9)) can be used to assess the electrical energy generated for a single thermal cycle. For example, F_E is related to the electrical energy (E) generated for a specific temperature change (ΔT), as shown in Fig. 2a, while F_E' relates to the electrical energy for a given thermal input, see Fig. 2b. Since power (P) is related to the energy generated per cycle (E) and frequency (f), where $P = Ef$, the maximum frequency of operation (f_{max}) is of interest; namely how fast the material can realistically be heated and cooled.

As an example, Pandya *et al.*[33] examined the pyroelectric power density when operating a thermal cycling frequencies in the range of 10–2000 Hz. The maximum operating frequency to achieve thermal cycling is likely to be related to the heat transfer properties of the material, which are rarely included in the F_E and F_E' figures of merit outlined above. We now derive new figures of merit to take this into account based on the two modes of operation in Fig. 2.

Let us consider a pyroelectric material exposed to a heat source or radiation at a power density W (J s^{-1} m^{-2}), that is modulated at a frequency (f). The heat is absorbed by the surface of the material, leading to an increase in temperature. For the energy harvesting figures of merit outlined above (eqn (8) and (9)), it is often assumed that the thermal energy is absorbed rapidly and is homogenously distributed throughout the volume of the pyroelectric, resulting in a uniform temperature change (ΔT). For example, for F_E, the material is cycled between two temperatures T_1 and T_2, and assumed to have attained thermal equilibrium. Likewise, F_E' relates to the

electrical energy for a given thermal input, leading to a uniform temperature change (ΔT) throughout the whole volume of the pyroelectric.[32]

However, to achieve a uniform change in temperature throughout the pyroelectric, it is important to establish a thermal equilibrium between the pyroelectric and the heat source. The need for a state of thermal equilibrium has an impact on the frequency of temperature cycles, the rate of heating, and the time intervals between temperature changes. As a result, it is important to recognise that it takes a finite time for the material to reach thermal equilibrium, which determines how quickly the material can respond to a fluctuating heat source. This in turn impacts the maximum frequency of thermal changes, and the maximum power output since $P_{max} = Ef_{max}$.

In this regard, we can take inspiration from heating concepts that are used to undertake pyroelectric measurements, where homogeneous heating of the sample under test is also a requirement for precise measurement of the pyroelectric coefficient (p). The time required to establish a thermal equilibrium between the pyroelectric sample and a heat source determines the excitation frequency, heating rate, or duration between the temperature cycles. Jachalke *et al.*[26] have provided a detailed overview of methods to undertake pyroelectric measurements, where the maximum thermal excitation frequency to achieve homogeneous heating of a pyroelectric element of thickness, t, is achieved at the condition $\omega = 2\frac{K}{t^2}$, where ω is the angular frequency, $K = \frac{\lambda}{\rho c_p}$ is the thermal diffusivity, λ is the thermal conductivity, ρ is the mass density and c_p is the specific heat capacity. Thus, the maximum thermal excitation frequency can be written as[26,34]

$$f_{max} \ll \frac{\omega}{2\pi} = \frac{K}{\pi t^2} = \frac{\lambda/\rho c_p}{\pi t^2} = \frac{\lambda}{\pi c_E t^2}. \quad (10)$$

This maximum frequency is derived based on the assumption that the sample is heated on both sides to achieve thermal equilibrium. Jachalke *et al.*[26] has also provided a detailed evaluation of single-sided heating, leading to a f_{max} that is four times smaller. Eqn (10) implies that for thermal energy harvesting *via* thermal cycling, (i) bulk pyroelectric materials, which have a large t, face limitations in terms of operating at high frequencies since it takes longer to change the temperature and reach thermal equilibrium throughout the material; (ii) pyroelectric thin film materials, which have a low t, have potential to be cycled at high frequencies, since they will take short time to reach thermal equilibrium;[34] for example, thin films with a large surface diameter and small thickness (t) can achieve maximum cycling frequencies in the kHz range;[26] and (iii) pyroelectric materials with a low thermal diffusivity (K) also have a limit on their ability to be rapidly thermally cycled. While a low thermal diffusivity is desirable for thermal sensing since it reduces unwanted lateral diffusion (see eqn (6)), a high thermal diffusivity is therefore preferable for rapid thermal cycling for energy harvesting since it facilitates a higher operating frequency, or allows a larger thickness (and therefore volume) of pyroelectric material to be employed when operating at specific frequency.[35]

In terms of heat transfer properties, semiconductors, where electron transport dominates thermal conduction (as opposed to phonons in insulators[36]) can exhibit high thermal conductivity and diffusivity, although dielectric losses may increase. Single crystals, which are characterized by long-range atomic order,[37] also facilitate efficient heat transfer. The inherent structure of 2D materials is also attractive since it enables efficient heat transfer as a result of surface scattering that alters the contribution of phonons with long mean free paths.[38] In contrast, bulk polycrystalline ceramics can lead to strong phonon localization, thereby reducing the thermal conductivity.[39] Similarly, materials incorporating nanoscale electrically insulating dopants exhibit a low thermal conductivity and diffusivity as a result of defect scattering, which can hinder heat transfer and impede achieving thermal equilibrium.[36,39] Polymers and polymer-derived composites can also contain air-filled gaps, voids, or interfaces, resulting in a significant interfacial thermal resistance across any contacting surfaces, thereby limiting heat transfer.[40]

While eqn (10) indicates that the search for materials with low volumetric heat capacity ($c_E = \rho c_p$) is beneficial, this property tends to be relatively consistent across different materials as a result of the Dulong-Petit law,[41] which states that the molar heat capacity of a solid is equal to approximately $3R$, where R is the gas constant.[42] As a result, low thickness and high thermal conductivity are the most important criteria for maximizing the thermal excitation frequency.

Based on this knowledge, we can now introduce two new figures of merit to generate a large amount of energy per cycle (E) while also enabling high-frequency heating and cooling (a high f_{max}) to produce a high-power output, since $P_{max} = Ef_{max}$. First, we consider a pyroelectric energy harvesting element undergoes a temperature change from T_1 to T_2 by placing a pyroelectric material in thermal contact with a cold and a hot source, as in Fig. 2a.[17,19]

The temperature change is given by:

$$\Delta T = T_2 - T_1 \quad (11)$$

When a pyroelectric is subjected to a temperature change (ΔT), the charge (ΔQ) released by the area (A) of pyroelectric material due to a change in polarisation is given by,

$$\Delta Q = pA\Delta T \quad (12)$$

It is evident from eqn (12) that the amount of pyroelectric charge can be optimized by increasing the area (and the corresponding screening charge, Fig. 1b), increasing the pyroelectric coefficient (the change in polarisation), or having a large change in temperature.

The pyroelectric element can be considered as a parallel plate capacitor with conducting electrodes of area A on either side of a dielectric pyroelectric material with a thickness, t, as shown in Fig. 1. The capacitance, C, of the pyroelectric element is given by:

$$C = \frac{A\varepsilon_{33}^{\sigma}}{t} \tag{13}$$

Since the charge (Q) is correlated with the capacitance (C) and voltage (V) by $Q = CV$, the open circuit voltage, V_{OC}, generated due to the temperature change can be written as:

$$V_{OC} = \frac{Q}{C} = \frac{pt\Delta T}{\varepsilon_{33}^{\sigma}} \tag{14}$$

Eqn (14) indicates that the open circuit voltage, V_{OC}, can be increased by increasing the thickness of the pyroelectric element, the pyroelectric coefficient, and the temperature change, or by reducing the permittivity of the material.

For energy harvesting applications, we are interested in the electrical energy (E) produced and stored in the parallel plate capacitor of capacitance of C, which can be written as $E = \frac{1}{2}CV^2$, so that,

$$E = \frac{1}{2}\frac{p^2}{\varepsilon_{33}^{\sigma}}(\Delta T)^2 At \tag{15}$$

It can be seen that the pyroelectric charge (eqn (12)), open circuit voltage (eqn (14)), and energy per thermal cycle (eqn (15)) are independent of frequency and are simply a function of the temperature change (ΔT), while the short circuit current (eqn (2)) is a function of the rate of change of temperature (dT/dt) and is dependent on the frequency of the thermal cycle. Whatmore[16] has provided an excellent overview and discussion of the analysis of pyroelectric detectors, and their frequency dependence, on considering both the thermal and electrical circuits.

Based on eqn (15), the corresponding energy density (energy per unit volume) for a single thermal cycle, can therefore be written as:

$$\frac{E}{At} = \frac{1}{2}\frac{p^2}{\varepsilon_{33}^{\sigma}}(\Delta T)^2 \tag{16}$$

This leads to the pyroelectric energy harvesting figure of merit, F_E, that maximises the energy produced for a given temperature change ΔT and volume of material (At):[26,32–35]

$$F_E = \frac{p^2}{\varepsilon_{33}^{\sigma}} \tag{17}$$

However, based on a maximum operating frequency (f_{max}) where the materials can be cycled between T_1 and T_2, the maximum power (P_{max}) is:

$$P_{max} = Ef_{max} \tag{18}$$

Therefore, while the energy (E) per thermal cycle (eqn (15)) is independent of the temperature change, since power (eqn (18)) is related to the number of cycles per unit time, it is advantageous to achieve high-frequency thermal oscillations, where f_{max} is given by eqn (10).

Using eqn (10), (15) and (18) the maximum achievable power density when attempting to cycle the pyroelectric element between a given hot and cold temperature source is,

$$\frac{P_{max}}{At} = \frac{1}{2}\frac{p^2}{\varepsilon_{33}^{\sigma}}\frac{\lambda(\Delta T)^2}{\pi\rho c_p t^2} = \frac{1}{2}\frac{p^2}{\varepsilon_{33}^{\sigma}}\frac{\lambda(\Delta T)^2}{\pi c_E t^2} \tag{19}$$

If we consider the case for a pyroelectric energy harvester with a specific surface area A and thickness t, that is subjected to a specific temperature change ΔT, the maximum power output can be expressed by a new figure of merit, which is termed the *first pyroelectric power figure of merit*, F_{P1}, as defined as:

$$F_{P1} = \frac{p^2}{\varepsilon_{33}^{\sigma}}\frac{\lambda}{\rho c_p} = \frac{p^2}{\varepsilon_{33}^{\sigma}}\frac{\lambda}{c_E} \tag{20}$$

This figure of merit can also be written in terms of the thermal diffusivity (K) as:

$$F_{P1} = \frac{p^2}{\varepsilon_{33}^{\sigma}}K \tag{21}$$

Therefore, in the mode of thermal harvesting in Fig. 2a there is benefit in using materials with a combination of a high pyroelectric coefficient (to enhance the charge generated), a low permittivity (to increase the output voltage) and a high thermal diffusivity (to increase the maximum operational frequency).

In addition to harvesting between two distinct temperature sources (T_1 and T_2), there may also be energy harvesters that are subject to an oscillating/modulating thermal energy source. An example of this approach involves varying the temperature by using a heating lamp, or sunlight, as a radiation source that is combined with a rotating disc chopper to periodically heat a pyroelectric element.[43–45]

In this configuration, the system directly harnesses a fluctuating/modulated thermal source, as illustrated in Fig. 2b, and the temperature increase of the pyroelectric is dependent on the volumetric specific heat. For example, if a pyroelectric material is exposed to radiation of power density W (J s^{-1} m^{-2}) for a time, Δt, radiation is absorbed onto the surface of the material and results in an increase in the temperature, ΔT. If we assume that the radiation absorbed is evenly distributed throughout the pyroelectric element, there is a uniform temperature increase. Neglecting heat losses from the pyroelectric, the increase in temperature is related to incident power density by,

$$\Delta T = \frac{W\Delta t}{c_p\rho t} = \frac{W\Delta t}{c_E t} \tag{22}$$

Based on this assumption, the F_E' figure of merit (eqn (9)) determines the energy density for a single cycle when harvesting in such a configuration. This concept can also be combined with the maximum frequency of operation (f_{max}) based on a homogeneous temperature, defined by eqn (10), to provide a new figure of merit based on ability to generate power for a modulated thermal input:

$$P_{max} = Ef_{max} \propto F_E' f_{max} \propto F_E' \frac{\lambda}{c_E l^2} \quad (23)$$

This leads to a *second pyroelectric power figure of merit*, F_{P2}

$$F_{P2} = \frac{p^2 \lambda}{\varepsilon_{33}^{\sigma} {c_E}^3} \quad (24)$$

In terms of thermal diffusivity (K), the dynamic pyroelectric power figure of merit is given by:

$$F_{P2} = \frac{p^2 K}{\varepsilon_{33}^{\sigma} {c_E}^2} \quad (25)$$

Both F_{P1} (eqn (21)) and F_{P2} (eqn (25)) represent two new pyroelectric power figures of merit for the selection and design of materials for pyroelectric energy harvesters. The new figures of merit are of interest for the selection of materials, and the design of pyroelectric materials for thermal harvesting devices. They provide guidance for the development of novel materials and composites for pyroelectric energy harvesting applications, in particular when there is a need for rapid thermal cycling to increase the frequency of operation and power output, depending on the mode of operation, as outlined in Fig. 2.

3.1 Materials selection based on new power figures of merit (F_{P1} and F_{P2})

Table 1 outlines the range of relevant properties for a variety of pyroelectric materials, which includes the relevant pyroelectric material properties (p, $\varepsilon_{33}^{\sigma}$, ρ, c_E, c_p, λ and K) and a range of pyroelectric figures of merit for sensing (F_v and F_i), energy harvesting (F_E and F_E') and the two new power-related figures of merit (F_{P1} and F_{P2}). Table 1 provides the materials parameters and corresponding figures of merit of ceramics, semiconductors, single crystals, thin film, polymers, composites and 2D pyroelectric materials.

Ashby materials selection charts have been produced to provide a visual representation of the data in Table 1. This is achieved by taking logarithms and selecting specific properties for the x- and y-axes and has been recently used for F_v (eqn (3)) and F_D (eqn (5)).[46]

From eqn (21), for the selection of materials with high F_{P1} when thermally cycling between two temperature sources T_1 and T_2, this leads to:

$$\log\left(\frac{p^2}{\varepsilon_{33}^{\sigma}}\right) = \log(F_E) = -\log(K) + \log(F_{P1}) \quad (26)$$

Therefore, on a log–log graph where F_E is the y-axis and thermal diffusivity (K) is the x-axis, it is possible to produce lines of constant F_{P1}, by placing a line of gradient $n = -1$ on the chart, as shown in Fig. 3a.

From eqn (25), for the selection of materials with high F_{P2}, when harvesting a modulated thermal input, this leads to:

$$\log\left(\frac{p^2}{\varepsilon_{33}^{\sigma} {c_E}^2}\right) = \log\left(F_E'\right) = -\log(K) + \log(F_{P2}) \quad (27)$$

Likewise, on a log–log graph with F_E' on the y-axis and thermal diffusivity (K) on the x-axis, it is possible to draw lines of constant F_{P2} by placing a line of gradient $n = -1$ on the chart, as in Fig. 3b.

There are no significant changes in order or relative location of materials in the Ashby charts in Fig. 3a and b, which is a result of the relatively small variation in volumetric specific heat between the range of materials in the literature; see Table 1. The polymeric ferroelectric materials have relatively low F_{P1} and F_{P2}, due to the low thermal diffusivity and low pyroelectric coefficients (Fig. 3 and Table 1). The pyroelectric semiconductor materials (GaN and AlN) have a high thermal diffusivity but relatively low F_{P1} and F_{P2} due to their low pyroelectric coefficients. Polycrystalline ferroelectric materials (PZT, PLZT and $BaTiO_3$) exhibit relatively high F_{P1} and F_{P2} due to their high pyroelectric coefficients and intermediate values of thermal diffusivity. The single-crystal and thin-film materials ($LiTaO_3$, $LiNbO_3$, HfO_2, and PMN-PT) are of interest since they exhibit high pyroelectric coefficients and relatively high thermal diffusivity. The composite materials perform relatively well, see both Fig. 3 and Table 1; composites are of interest since they provide a route to tailor the pyroelectric, dielectric and heat transfer properties. Composites could be developed to combine a material with high pyroelectric coefficient and a high thermal conductivity; for example, Wang *et al.* explored the potential of ferroelectric ceramics that contain a thermally conductive network with AlN or BN nanoparticles for thermal harvesting applications.[24,47]

Recently, two-dimensional pyroelectric materials have attracted interest in waste thermal energy harvesting.[48] There is evidence that such materials can exhibit large thermal conductivities, up to 500 W m^{-1} K^{-1},[49] although less work has aimed at producing both thermal properties and pyroelectric coefficient, and is a potential topic of future interest. The 2D few-layer black phosphorus material in Fig. 3 and Table 1 indicates potential to achieve a very high F_{P1} and F_{P2} values due to a combination of a high pyroelectric coefficient and high thermal diffusivity.

Interestingly, external factors can also have an impact on the heat transfer properties. Shekhan *et al.*[50] indicated a difference in the thermal conductivity of a pyroelectric in the poling direction depending on whether the materials was under a short-circuit (λ_{33}^{E}), open-circuit (λ_{33}^{D}) and unpoled (λ^{u}) condition, whereby $\lambda_{33}^{E} > \lambda_{33}^{D} > \lambda^{u}$. This indicates the mode of operation of a pyroelectric can have on influence on thermal response. Changes in the thermal conductivity of ferroelectrics have also been linked to variations in the piezoelectric coefficient,[51] applied electric field[52] and light.[53]

In addition to the figures of merit, the equations above can also indicate simple geometric considerations for thermal energy harvesting. Clearly, there is a need to maximise the active area (A) of the pyroelectric to maximise the amount of surface charge, see eqn (12) and Fig. 1. While a large volume (At) is desirable to maximise the amount of electrical energy produced in a single cycle, see eqn (15), the pyroelectric should be as thin as possible to maximise the frequency of operation by reducing the time required to establish thermal equilibrium between the pyroelectric sample and the heat source, see eqn (10). While the two new figures of merit (eqn (21) and (25)), have been derived

Table 1 Pyroelectric materials with key parameters and figures of merit (FoMs); ε_r is relative permittivity. References to source of materials property are indicated in final column, unless otherwise stated

Material and class	$\lvert p\rvert$ ($\times 10^{-6}$ C m^{-2} K^{-1})	ε_r	ρ (kg m^{-3})	c_p (J kg^{-1} K^{-1})	c_E ($\times 10^6$ J m^{-3} K^{-1})	λ (W m^{-1} K^{-1})	K ($\times 10^{-7}$ m^2 s^{-1})	F_i ($\times 10^{-12}$ m V^{-1})	F_v (m^2 C^{-1})	F_E (J m^{-3} K^{-2})	F_E' ($\times 10^{-12}$ m^3 J^{-1})	F_{P1} ($\times 10^{-6}$ W m^{-1} K^{-2})	F_{P2} ($\times 10^{-18}$ m^5 J^{-1} s^{-1})	Ref.
PZT-5H ceramic	533 (ref. 27)	1116 (ref. 27)	7600	340	2.58	1.4 (ref. 50)	5.4	206.6	0.02	28.76	4.13	15.53	2.33	50
$BaTiO_3$ ceramic	800 (ref. 54)	2350	5710	360	2.06 (ref. 54)	6.0 (ref. 55)	29.1	388.3	0.019	30.77	7.37	89.54	21.1	54 and 55
PLZT ceramic	1200 (ref. 55)	4285	6307	418.6	2.64 (ref. 55)	0.77	2.9 (ref. 56)	454.5	0.012	37.97	5.45	11.01	1.58	55 and 56
AlN semiconductor	5.0	9.1	5250	600	3.15	285 (ref. 57)	904.8	1.59	0.02	0.31	0.03	28.05	2.83	55 and 57
GaN semiconductor	5.3	10.4	6428	490	3.15	130 (ref. 57)	412.7	1.68	0.018	0.305	0.03	12.59	1.27	55 and 57
0.75PMN-0.25 PT single crystal	1790	961	—	—	2.5	1.43 (ref. 58)	5.7	716	0.0844	376.95	60.14	214.86	34.38	25
$LiNbO_3$ single crystal	72	31.4	4652	627.6	2.92	5.6	19.2	24.66	0.089	18.65	2.19	35.81	4.19	55
$LiTaO_3$ single crystal	180	47	—	—	3.2	4.6	14.37	56.25	0.135	77.89	7.59	111.93	10.93	59
PVDF polymer	25	9	1740 (ref. 58)	1322	2.3	0.22	0.956	10.87	0.136	7.85	1.48	0.75	0.14	55 and 60
PVDF–TrFE polymer	35	8	1900 (ref. 60)	1211	2.3	0.22	0.956	15.22	0.215	17.30	3.27	1.65	0.31	55 and 60
HfO_2 thin film	46.2	31.5	—	—	2.63	14.1 (ref. 61)	53.6	17.55	0.063	7.64	1.11	40.96	5.92	61 and 62
PMN-PMS-PZT:0.2AlN	4146	5357	6300	284	1.79	0.70	3.9	2316.2	0.049	362.6	113.49	142.5	44.47	24
PMN-PMS-PZT:0.1BN	3423	5730	6810	285	1.94	0.895	4.6	1764.4	0.035	231.06	61.75	106.52	28.3	47
2D-BP	5287 (ref. 63)	8.3 (ref. 64)	2690 (ref. 65)	800 (ref. 66)	2.15	40 (ref. 67)	186	2459.1	33.48	0.38×10^6	0.08×10^6	7.08×10^6	1.53×10^6	63–67
In_2Se_3	5500 (ref. 68)	17 (ref. 69)	—	—	1.4 (ref. 70)	60 (ref. 71)	428.6	3928.6	26.1	0.2×10^6	0.1×10^6	8.57×10^6	4.372×10^6	68–71

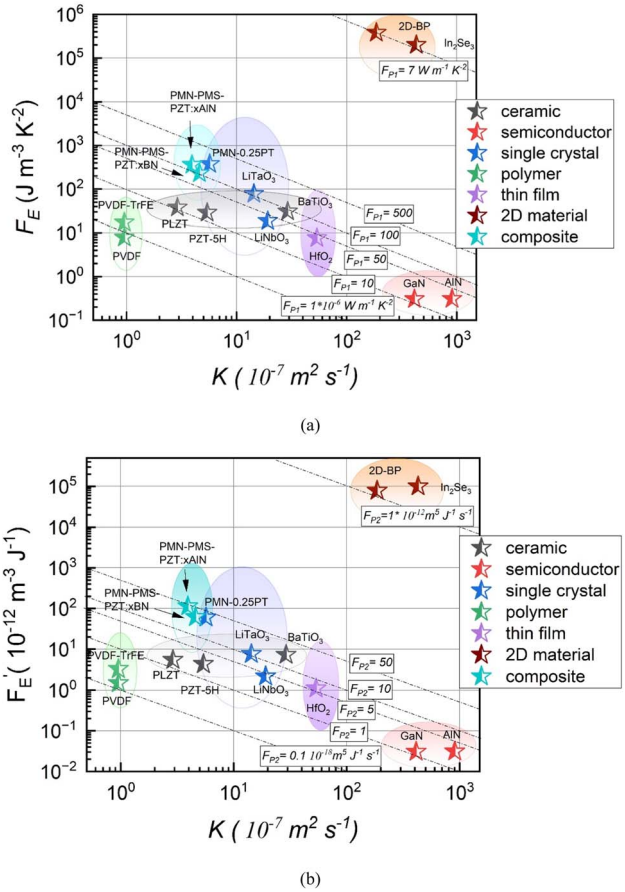

Fig. 3 Ashby charts. (a) Selection of materials with high $F_{P1} = F_E K$, lines of constant F_{P1} can be drawn *via* a gradient of $n = -1$, based on eqn (26). (b) Selection of materials with high $F_{P2} = F_E' K = F_{P1}/c_E^2$, lines of constant F_{P2} can be drawn *via* a gradient of $n = -1$, based on eqn (27).

based on attempting to maximise the thermal excitation frequency (f_{max}) for a pyroelectric element with a specific thickness, it is also of interest to consider thermal harvesting of a heat source that is fluctuating at a specific frequency, f. In this case, a high thermal diffusivity material enables homogeneous heating of pyroelectric element of larger thickness (eqn (10)), and therefore volume, to increase the energy per cycle; for example, when thermal cycles are provided by a rotating disc chopper rotating at a constant speed.[45] From eqn (10) it can be seen that the maximum thickness (t_{max}) is given by $t_{max} = (K/\pi f)^{0.5}$, and this leads to a modified figure of merit, $F_{P3} = \frac{p^2}{\varepsilon_{33}^{\sigma}} K^{0.5}$; a full derivation of this figure of merit, and F_{P1}, are included in the supplemental material. There is potential to produce Ashby diagrams that include both materials properties and shape-factors for optimising the material-and-shape combination.[72]

4. Conclusions

This paper has outlined new performance figures of merit for the selection and design of pyroelectric materials for harvesting dynamic temperature fluctuations. These new figures of merit are able to assist in selection of the most suitable pyroelectric materials for optimal power output while harvesting thermal cycles for a range of thermal cycles. According to these new criteria, materials for thermal harvesting should exhibit (i) a high pyroelectric coefficient to maximise the generated charge for a given change in temperature (ΔT), (ii) a low permittivity to maximise the voltage and electrical energy for a given charge (eqn (14) and (15)), (iii) a high thermal diffusivity or thermal conductivity to maximise the operational frequency by reducing the time required to establish a thermal equilibrium (eqn (10)), and (iv) a low heat capacity to maximise the temperature change, when the pyroelectric is subjected to a varying thermal input; however, for many materials this parameter is similar as a result of the Dulong–Petit law.[42] A clear route to increase the power output significantly is therefore to design, or discover, new materials with this attractive combination of properties. The analysis here also provides guidelines for geometric considerations where the pyroelectric should be as thin as possible, to maximise the frequency of operation, but of high active area to maximise the amount of charge generated. A high thermal diffusivity also enables a pyroelectric element with a larger thickness, and therefore volume, to be employed when a thermal cycle is at a specific frequency. The new figures of merit therefore provide a quantitative approach for the selection and design of materials where composites, single crystal-like and emerging two-dimensional pyroelectrics appear particularly attractive as a route to produce materials with a unique combination of high pyroelectric activity and high heat transfer properties.

Data availability

The data supporting this article have been included as references.

Author contributions

Bastola Narayan: writing of the original draft, conceptualization, analysis, methodology and investigation, editing, review. Qingping Wang: writing of the original draft, conceptualization, methodology, data collection and investigation, editing, review. James Roscow: editing, review. Chaoying Wan: editing, review. Chris Bowen: conceptualization, methodology, supervision, analysis, writing of the original draft, editing, review.

Conflicts of interest

There are no conflicts to declare.

Acknowledgements

BN and CB acknowledge support of UKRI Frontier Research Guarantee on "Processing of Smart Porous Electro-Ceramic Transducers – ProSPECT", Project No. EP/X023265/1. QW acknowledges support of UKRI Postdoctoral Fellowship

Guarantee (Project No. EP/Y017412/1), and the National Natural Science Foundation of China (Project No. 51902094).

References

1 C. R. Bowen, J. Taylor, E. LeBoulbar, D. Zabek, A. Chauhan and R. Vaish, *Energy Environ. Sci.*, 2014, **7**, 3836–3856.
2 P. Lheritier, A. Torello, T. Usui, Y. Nouchokgwe, A. Aravindhan, J. Li, U. Prah, V. Kovacova, O. Bouton, S. Hirose and E. Defay, *Nature*, 2022, **609**, 718–721.
3 Q. Q. Wu, Y. Zhao and X. C. Li, *Sens. Actuators, A*, 2024, **367**, 115050.
4 L. Kouchachvili and M. Ikura, *Int. J. Energy Res.*, 2008, **32**, 328–335.
5 I. M. McKinley, S. Goljahi, C. S. Lynch and L. Pilon, *J. Appl. Phys.*, 2013, **114**, 224111.
6 A. Navid and L. Pilon, *Smart Mater. Struct.*, 2011, **20**, 025012.
7 Q. Wang, Q. Sun, Z. Xu, H. Luo, S. Li and T. Wu, *Surf. Interfaces*, 2024, **51**, 104657.
8 S. Jachalke, E. Mehner, H. Stöcker, J. Hanzig, M. Sonntag, T. Weigel, T. Leisegang and D. C. Meyer, *Appl. Phys. Rev.*, 2017, **4**, 021303.
9 R. Whatmore, in *Characterisation of Ferroelectric Bulk Materials and Thin Films*, ed. M. G. Cain, Springer Netherlands, Dordrecht, 2014, pp. 65–86.
10 S. B. Lang, *Phys. Today*, 2005, **58**, 31–36.
11 J. D. Brownridge, *Nature*, 1992, **358**, 287–288.
12 S. Mohtashami, H. Afarideh and K. Moshkbar-Bakhshayesh, *J. Appl. Phys.*, 2024, **135**, 200701.
13 E. Gutmann, A. Benke, K. Gerth, H. Böttcher, E. Mehner, C. Klein, U. Krause-Buchholz, U. Bergmann, W. Pompe and D. C. Meyer, *J. Phys. Chem. C*, 2012, **116**, 5383–5393.
14 A. Kakekhani and S. Ismail-Beigi, *J. Mater. Chem. A*, 2016, **4**, 5235–5246.
15 Z. Kutnjak, B. Rožič and R. Pirc, in *Wiley Encyclopedia of Electrical and Electronics Engineering*, John Wiley & Sons, Ltd, 2015, pp. 1–19.
16 R. W. Whatmore, *Rep. Prog. Phys.*, 1986, **49**, 1335.
17 F. Y. Lee, A. Navid and L. Pilon, *Appl. Therm. Eng.*, 2012, **37**, 30–37.
18 Q. Leng, L. Chen, H. Guo, J. Liu, G. Liu, C. Hu and Y. Xi, *J. Mater. Chem. A*, 2014, **2**, 11940–11947.
19 M. Shiran Chaharsoughi, D. Tordera, A. Grimoldi, I. Engquist, M. Berggren, S. Fabiano and M. P. Jonsson, *Adv. Opt. Mater.*, 2018, **6**, 1701051.
20 J. P. Feser and J. Ravichandran, *Nat. Mater.*, 2018, **17**, 385–386.
21 C. S. Wei, Y. Y. Lin, Y. C. Hu, C. W. Wu, C. K. Shih, C. T. Huang and S. H. Chang, *Sens. Actuators, A*, 2006, **128**, 18–24.
22 D. Zabek, J. Taylor, E. L. Boulbar and C. R. Bowen, *Adv. Energy Mater.*, 2015, **5**, 1401891.
23 Q. Wang, C. R. Bowen and V. K. Valev, *Adv. Funct. Mater.*, 2024, **34**, 2312245.
24 Q. Wang, C. R. Bowen, W. Lei, H. Zhang, B. Xie, S. Qiu, M.-Y. Li and S. Jiang, *J. Mater. Chem. A*, 2018, **6**, 5040–5051.
25 Q. Wang, X. Zhang, C. R. Bowen, M.-Y. Li, J. Ma, S. Qiu, H. Liu and S. Jiang, *J. Alloys Compd.*, 2017, **710**, 869–874.
26 S. Jachalke, E. Mehner, E. Mehner, H. Stöcker, J. Hanzig, M. Sonntag, T. Weigel, T. Leisegang and D. C. Meyer, *Appl. Phys. Rev.*, 2017, **4**, 021303.
27 G. Sebald, E. Lefeuvre and D. Guyomar, *IEEE Trans. Ultrason. Ferroelectrics Freq. Control*, 2008, **55**, 538–551.
28 G. Sebald, L. Seveyrat, D. Guyomar, L. Lebrun, B. Guiffard and S. Pruvost, *J. Appl. Phys.*, 2006, **100**, 124112.
29 R. V. K. Mangalam, J. C. Agar, A. R. Damodaran, J. Karthik and L. W. Martin, *ACS Appl. Mater. Interfaces*, 2013, **5**, 13235–13241.
30 S. K. T. Ravindran, T. Huesgen, M. Kroener and P. Woias, *Appl. Phys. Lett.*, 2011, **99**, 104102.
31 A. Navid, C. S. Lynch and L. Pilon, *Smart Mater. Struct.*, 2010, **19**, 055006.
32 C. R. Bowen, J. Taylor, E. Le Boulbar, D. Zabek and V. Yu. Topolov, *Mater. Lett.*, 2015, **138**, 243–246.
33 S. Pandya, J. Wilbur, J. Kim, R. Gao, A. Dasgupta, C. Dames and L. W. Martin, *Nat. Mater.*, 2018, **17**, 432–438.
34 C. Dias, M. Simon, R. Quad and D. K. Das-Gupta, *J. Phys. D: Appl. Phys.*, 1993, **26**, 106.
35 D. Zhang, H. Wu, C. R. Bowen and Y. Yang, *Small*, 2021, **17**, 2103960.
36 G. Burns. *Solid State Physics*; Academic Press, Inc., 1985, pp: 433–441.
37 **https://www.sciencedirect.com/topics/engineering/thermal-equilibrium**.
38 Z. Luo, J. Maassen, Y. Deng, Y. Du, R. P. Garrelts, M. S. Lundstrom, P. D. Ye and X. Xu, *Nat. Commun.*, 2015, **6**, 8572.
39 R. J. Balsano, Thermal Conductivity Measurement of $(TiO2)_{1-x}(HfO2)_x$, Master thesis, Binghamton University, 2007.
40 X. Xu, J. Chen, J. Zhou and B. Li, *Adv. Mater.*, 2018, **30**, 1705544.
41 Y. Qizhen, Z. Zhang, G. Haibo and W. Yang, Physical properties and effect of helium-vacancy pair on tungsten/graphene composite as plasma-facing materials from first principles, *Fusion Sci. Technol.*, 2023, **80**, 178–195.
42 L. D. Landau and E. M. Lifshitz, *Statistical Physics Pt. 1. Course in Theoretical Physics*: Pergamon Press, Oxford, 3rd edn, 1980, vol. 5, pp. 193–196.
43 P. Mane, J. Xie, K. K. Leang and K. Mossi, *IEEE Trans. Ultrason. Ferroelectrics Freq. Control*, 2011, **58**, 10–17.
44 M. Xie, D. Zabek, C. Bowen, M. Abdelmageed and M. Arafa, *Smart Mater. Struct.*, 2016, **25**, 125023.
45 S. H. Krishnan, D. Ezhilarasi, G. Uma and M. Umapathy, *IEEE Trans. Sustain. Energy*, 2014, **5**, 73–81.
46 M. Ashby, T. Davies and S. Gorsse, *The CES EduPack DB for Bulk Functional Materials*, 2015, pp. 1–45, **https://www.teachingresources.grantadesign.com**.
47 Q. Wang, C. R. Bowen, R. Lewis, J. Chen, W. Lei, H. Zhang, M.-Y. Li and S. Jiang, *Nano Energy*, 2019, **60**, 144–152.
48 A. Kumar and D. Mandal, *Adv. Energy Mater.*, 2024, **14**, 2403319.
49 B. Mortazavi, B. Javvaji, F. Shojaei, T. Rabczuk, A. V. Shapeev and X. Zhuang, *Nano Energy*, 2021, **82**, 105716.

50 H. N. Shekhan, E. A. Gurdal, L. Ganapatibhotla, J. K. Maranas, R. Staut and K. Uchino, *Insight - Mater. Sci.*, 2020, **3**, 10.
51 D. Rashadfar, B. L. Wooten and J. P. Heremans, *arXiv*, 2025, preprint, arXiv:2402.08516, DOI: **10.48550/arXiv.2402.08516**.
52 C. Liu, Z. Chen, C. Wu, J. Qi, M. Hao, P. Lu and Y. Chen, *ACS Appl. Mater. Interfaces*, 2022, **14**, 46716–46725.
53 C. Cazorla, S. Bichelmaier, C. Escorihuela-Sayalero, J. Íñiguez, J. Carrete and R. Rurali, *Nanoscale*, 2024, **16**, 8335–8344.
54 K. K. Deb, M. D. Hill and J. F. Kelly, *J. Mater. Res.*, 1992, **7**, 3296–3305.
55 S. Jachalke, Characterization of Novel Pyroelectrics: From Bulk to Thin Film HfO_2, PhD thesis, Technische Universität Bergakademie Freiberg, 2019.
56 T. H. Lin, D. Edwards, R. E. Reedy, K. Das, W. McGinnis and S. H. Lee, *Ferroelectrics*, 1988, **77**, 153–160.
57 *NSM Archive - Aluminium Nitride (AlN) - Thermal properties*, **https://www.matprop.ru/AlN_thermal**, accessed January 20, 2025.
58 A. Negi, H. P. Kim, Z. Hua, A. Timofeeva, X. Zhang, Y. Zhu, K. Peters, D. Kumah, X. Jiang and J. Liu, *Adv. Mater.*, 2023, **35**, 2211286.
59 B. Ploss and S. Bauer, *Sens. Actuators, A*, 1991, **26**, 407–411.
60 R. d. Simoes, M. a. Rodriguez-Perez, J. a. De Saja and C. j. l. Constantino, *Polym. Eng. Sci.*, 2009, **49**, 2150–2157.
61 S. Zhang, S. Yi, J.-Y. Yang, J. Liu and L. Liu, *Int. J. Heat Mass Transfer*, 2023, **207**, 123971.
62 S. Jachalke, T. Schenk, M. H. Park, U. Schroeder, T. Mikolajick, H. Stöcker, E. Mehner and D. C. Meyer, *Appl. Phys. Lett.*, 2018, **112**, 142901.
63 H. You, Y. Jia, Z. Wu, F. Wang, H. Huang and Y. Wang, *Nat. Commun.*, 2018, **9**, 2889.
64 P. Kumar, B. S. Bhadoria, S. Kumar, S. Bhowmick, Y. S. Chauhan and A. Agarwal, *Phys. Rev. B*, 2016, **93**, 195428.
65 P. Chen, N. Li, X. Chen, W.-J. Ong and X. Zhao, *2D Mater.*, 2017, **5**, 014002.
66 Y. Aierken, D. Çakır, C. Sevik and F. M. Peeters, *Phys. Rev. B*, 2015, **92**, 081408.
67 Z. Luo, J. Maassen, Y. Deng, Y. Du, R. P. Garrelts, M. S. Lundstrom, P. D. Ye and X. Xu, *Nat. Commun.*, 2015, **6**, 8572.
68 J. Jiang, L. Zhang, C. Ming, H. Zhou, P. Bose, Y. Guo, Y. Hu, B. Wang, Z. Chen, R. Jia, S. Pendse, Y. Xiang, Y. Xia, Z. Lu, X. Wen, Y. Cai, C. Sun, G.-C. Wang, T.-M. Lu, D. Gall, Y.-Y. Sun, N. Koratkar, E. Fohtung, Y. Shi and J. Shi, *Nature*, 2022, **607**, 480.
69 D. Wu, A. J. Pak, Y. Liu, Y. Zhou, X. Wu, Y. Zhu, M. Lin, Y. Han, Y. Ren, H. Peng, Y.-H. Tsai, G. S. Hwang and K. La, *Nano Lett.*, 2015, **15**, 8136–8140.
70 H. Qi, C. Wu, P. Lu and C. Liu, *Nanotechnology*, 2024, **35**, 085701.
71 S. Zhou, X. Tao and Y. Gu, *J. Phys. Chem. C*, 2016, **120**, 4753–4758.
72 M. F. Ashby, *Acta Mater.*, 1991, **39**, 1025.